J|A|C|S
ARTICLES
Published on Web 03/02/2004

Fluorescence-Based Approach for Detecting and Characterizing Antibiotic-Induced Conformational Changes in Ribosomal RNA: Comparing Aminoglycoside Binding to Prokaryotic and Eukaryotic Ribosomal RNA Sequences

Malvika Kaul, Christopher M. Barbieri, and Daniel S. Pilch*

Contribution from the Department of Pharmacology, University of Medicine and Dentistry of New Jersey−Robert Wood Johnson Medical School, 675 Hoes Lane, Piscataway, New Jersey 08854-5635

Received October 1, 2003; E-mail: pilchds@umdnj.edu

Abstract: Aminoglycoside antibiotics bind specifically to a conserved sequence of the 16S ribosomal RNA (rRNA) A site and interfere with protein synthesis. One model for the mechanism underlying the deleterious effects of aminoglycosides on protein synthesis invokes a drug-induced conformational change in the rRNA that involves the destacking of two adenine residues (A1492 and A1493 in *Escherichia coli*) at the A site. We describe here a fluorescence-based approach for detecting and characterizing this drug-induced conformational change in the target rRNA. In this approach, we insert the fluorescent base analogue 2-aminopurine in place of A1492 in an *E. coli* 16S rRNA A-site model oligonucleotide (*Ec*WT) as well as in a mutant form of this oligomer (A1408G) in which A1408 has been replaced with a guanine. The presence of guanine at 1408 instead of adenine represents one of the major sequence differences between prokaryotic and eukaryotic A sites, with the latter A sites being resistant to the deleterious effects of aminoglycosides. Binding of the aminoglycoside paromomycin to the 2AP-substituted forms of *Ec*WT and A1408G induced changes in fluorescence quantum yield consistent with drug-induced base destacking in *Ec*WT but not A1408G. Isothermal titration calorimetry studies reveal that paromomycin binds to the *Ec*WT duplex with a 31-fold higher affinity than the A1408G duplex, with this differential affinity being enthalpic in origin. In the aggregate, these observations are consistent with both rRNA binding affinity and drug-induced base destacking being important determinants in the prokaryotic specificity of aminoglycosides. Combining fluorescence quantum yield and lifetime data allows for quantification of the extent of drug-induced base destacking, thereby providing a convenient tool for evaluating the relative impacts of both novel and existing A-site targeting ligands on rRNA conformation and potentially for predicting relative antibiotic activities and specificities.

Introduction

The antimicrobial activities of 2-deoxystreptamine (2-DOS) aminoglycoside antibiotics are derived from their deleterious impact on microbial protein synthesis, which includes mistranslation as well as translocation inhibition.[1] A key step toward achieving this biological end point is the specific binding to a conserved sequence in the 16S rRNA A site of the small ribosomal subunit. The molecular mechanism by which the specific aminoglycoside−rRNA recognition event results in aberrant translation has not been clearly delineated.

One model for this mechanism invokes a drug-induced conformational change in the rRNA.[2,3] Specifically, drug binding in the major groove of the rRNA A site causes the displacement of two conserved adenine residues (at positions 1492 and 1493 in *Escherichia coli* 16S rRNA) out of the helical stack toward the minor groove, wherein they interact with and stabilize the minihelix that is formed by the mRNA codon and the tRNA anticodon during the translation process. It is thought that even minihelices formed between *noncognate* anticodons and codons are stabilized in this manner, thereby giving rise to mistranslation effects. A number of recent biochemical and structural studies have lent support to this model for aminoglycoside-induced inhibition of protein synthesis.[2−7] Among the supporting structural data are the NMR-derived solution structures of an *E. coli* 16S rRNA A-site model oligonucleotide (PDB code 1A3M)[5] (*Ec*WT) (Figure 1A) and its complex with the aminoglycoside paromomycin (PDB code 1PBR)[4] (see Chart 1 for

* To whom correspondence should be addressed: Tel 732-235-3352; fax 732-235-4073.

(1) Puglisi, J. D.; Blanchard, S. C.; Dahlquist, K. D.; Eason, R. G.; Fourmy, D.; Lynch, S. R.; Recht, M. I.; Yoshizawa, S. In *The Ribosome: Structure, Function, Antibiotics, and Cellular Interactions*; Garrett, R. A., Douthwaite, S. R., Liljas, A., Matheson, A. T., Moore, P. B., Noller, H. F., Eds.; ASM Press: Washington, DC, 2000; pp 419−429.
(2) Yoshizawa, S.; Fourmy, D.; Puglisi, J. D. *Science* **1999**, *285*, 1722−1725.
(3) Carter, A. P.; Clemons, W. M.; Brodersen, D. E.; Morgan-Warren, R. J.; Wimberly, B. T.; Ramakrishnan, V. *Nature* **2000**, *407*, 340−348.
(4) Fourmy, D.; Recht, M. I.; Blanchard, S. C.; Puglisi, J. D. *Science* **1996**, *274*, 1367−1371.
(5) Fourmy, D.; Yoshizawa, S.; Puglisi, J. D. *J. Mol. Biol.* **1998**, *277*, 333−345.
(6) Vicens, Q.; Westhof, E. *Structure* **2001**, *9*, 647−658.
(7) Vicens, Q.; Westhof, E. *Chem. Biol.* **2002**, *9*, 747−755.

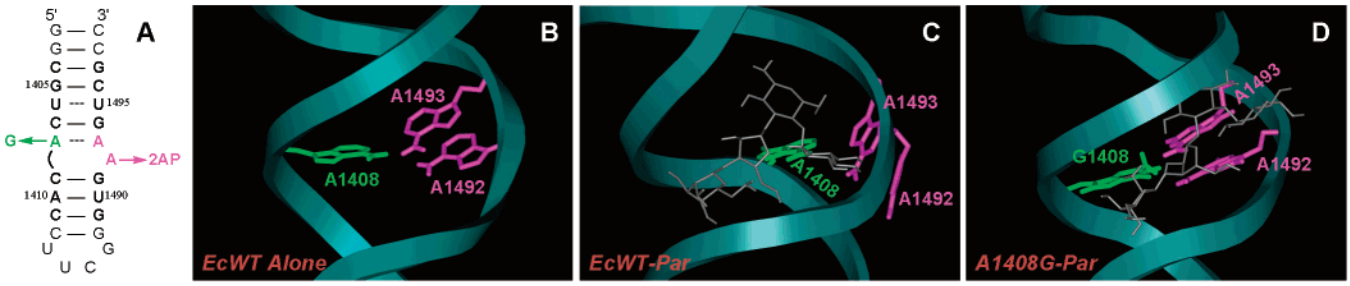

Figure 1. (A) Secondary structure of the *E. coli* 16S rRNA A-site model oligonucleotide (*Ec*WT). Bases present in *E. coli* 16S rRNA are depicted in boldface type and are numbered as they are in 16S rRNA. The bases at positions 1492 and 1493 are depicted in magenta, while the base at position 1408 is depicted in green. 2AP denotes 2-aminopurine. (B) Solution structure of *Ec*WT in the absence of drug.[5] The RNA backbone is depicted in ribbon format, with the color coding of the bases at positions 1408, 1492, and 1493 being as described above. (C) Solution structure of the paromomycin (Par)−*Ec*WT complex,[4] with the drug being depicted in gray. (D) Solution structure of paromomycin in complex with a mutated form of *Ec*WT in which the base at position 1408 is a guanine in place of adenine (A1408G).[8]

Chart 1. Structure of Paromomycin

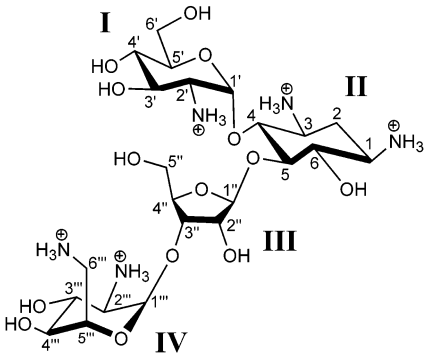

the chemical structure of paromomycin). A comparison of these structures, which are depicted in panels B and C of Figure 1, reveals the drug-induced destacking of A1492 and A1493 described above.

One of the key differences between the sequence of prokaryotic versus eukaryotic A sites is the identity of the base at position 1408 (by *E. coli* numbering), with this base being an adenine in prokaryotes and a guanine in eukaryotes. Figure 1D depicts a recently reported solution structure of paromomycin in complex with a mutant form of *Ec*WT in which the adenine residue at position 1408 is substituted with guanine (A1408G) (PDB code 1FYO).[8] Note that, in this complex, A1492 and A1493 are not destacked the way they are in the *Ec*WT−paromomycin complex (compare Figure 1 panels C and D), an observation suggesting that the abilities of aminoglycosides to induce a conformational change in the rRNA A site may be a key factor not only in their mechanism of action but also in their prokaryotic specificity of action.

Here, we describe a fluorescence-based approach for detecting and characterizing the aminoglycoside-induced conformational change in the A site of rRNA. This approach makes use of the fluorescent base analogue 2-aminopurine (2AP), which we have inserted into both *Ec*WT and A1408G in place of A1492. Hereafter, we refer to the 2AP-substituted forms of the *Ec*WT and A1408G duplexes as *Ec*WT(2AP) and A1408G(2AP), respectively. We selected A1492 as the base for 2AP substitution, since it is not engaged in any base pairing interactions (canonical or noncanonical) and its substitution should therefore be minimally perturbing to the RNA duplex. In a seminal set of solvent-dependent fluorescence studies, Ross and co-workers[9] have shown that the fluorescence of 2AP is modulated by hydrophobic stacking interactions and dynamic collisions with other bases, but not by hydrogen-bonding interactions. Thus, aminoglycoside-induced changes in the fluorescence of 2AP1492 provide a means for monitoring and quantifying the destacking of the base at position 1492 that accompanies drug−RNA complex formation.

Materials and Methods

RNA and Drug Molecules. All the 27mer RNA oligonucleotides used in this study were obtained in their polyacrylamide gel electrophoresis- (PAGE-) purified sodium salt forms from Dharmacon Research, Inc (Lafayette, CO). The extinction coefficient at 260 nm and 85 °C ($\epsilon_{260-85°C}$) for each of the RNA oligonucleotides was determined by colorimetric phosphate assay,[10] which resulted in the following values [in units of (moles [in strand]/liter)$^{-1}$·centimeter^{-1}]: $\epsilon_{260-85°C} = 253\,390 \pm 3170$ for *Ec*WT, $\epsilon_{260-85°C} = 248\,370 \pm 940$ for *Ec*WT(2AP), $\epsilon_{260-85°C} = 256\,760 \pm 4490$ for A1408G, and $\epsilon_{260-85°C} = 295\,400 \pm 3680$ for A1408G(2AP). Paromomycin·H_2SO_4 was obtained from Fluka.

UV Absorption Spectrophotometry. Temperature-dependent absorption experiments were conducted on an Aviv Model 14DS spectrophotometer (Aviv Biomedical; Lakewood, NJ) equipped with a thermoelectrically controlled cell holder. Quartz cells with a 1 cm path length were used for all the absorbance studies. Temperature-dependent absorption profiles were acquired at 274 nm with a 10 s averaging time. The temperature was raised in 0.5 °C increments, and the samples were allowed to equilibrate for 1 min at each temperature setting. In these UV melting studies, the RNA solutions were 2 μM in strand. When present, paromomycin was used at a concentration of 2 μM. Buffer solutions contained 10 mM sodium cacodylate (pH 5.5), 0.1 mM EDTA, and sufficient NaCl to bring the total sodium ion concentration to 60 mM.

Steady-State Fluorescence Spectroscopy. Steady-state fluorescence experiments were conducted on an Aviv Model ATF105 spectrofluorometer (Aviv Biomedical; Lakewood, NJ) equipped with a thermoelectrically controlled cell holder. A quartz cell with a 1 cm path length in both the excitation and emission directions was used in all the experiments, which were conducted at 25 °C. The RNA concentrations were 1 μM in strand. When present, paromomycin was used at a concentration of 1 μM, while guanidine hydrochloride was used at a concentration of 6 M. With the excitation wavelength set at 310 nm,

(8) Lynch, S. R.; Puglisi, J. D. *J. Mol. Biol.* **2001**, *306*, 1037−1058.

(9) Rachofsky, E. L.; Osman, R.; Ross, J. B. A. *Biochemistry* **2001**, *40*, 946−956.

(10) Plum, G. E. In *Current Protocols in Nucleic Acid Chemistry*; Beaucage, S. L., Bergstrom, D. E., Glick, G. D., Jones, R. A., Eds.; John Wiley & Sons: New York, 2000; Vol. 1, pp 7.3.1−7.3.17.

fluorescence emission spectra were acquired from 450 to 315 nm in 1 nm increments with an averaging time of 1 s. The excitation and emission slit widths were set at 3 and 4 nm, respectively. Buffer conditions were identical to those described above for the UV melting experiments.

Fluorescence quantum yield values (Φ) of *Ec*WT(2AP) and A1408G-(2AP) were determined relative to quinine sulfate in 1 N H_2SO_4, which was assigned a quantum yield of 0.546 at 25 °C.[11] For these determinations, RNA concentrations were 6 μM in strand, while the concentration of quinine sulfate was 5 μM. Fluorescence emission scans were acquired from 320 to 605 nm, with the excitation wavelength set to 310 nm. In these measurements, the quartz cell path lengths were 1 cm in the excitation direction and 0.2 cm in the emission direction. The excitation and emission slit widths were set at 3 and 4 nm, respectively.

Time-Resolved Fluorescence Spectroscopy. Time-resolved fluorescence experiments were conducted at 25 °C on a PTI LaserStrobe fluorescence lifetime spectrometer equipped with a thermoelectrically controlled cell holder. A PTI model GL-3300 nitrogen laser (at a 10 Hz frequency) was used to excite the samples at 337 nm and the fluorescence decay curves were acquired logarithmically at an emission wavelength of 370 nm (8 nm slit width) in 400 channels (with 5 laser shots/time point). The start and end delays of the acquisitions were 37 and 75 ns, respectively. The instrument response function was detected at 337 nm from light scattered by a dilute suspension of nondairy creamer. Each final decay profile reflected an average of 10 independent scans and was deconvolved in the Felix32 program (PTI, Inc.). Goodness of fit was judged on the basis of a reduction in χ^2 and inspection of the autocorrelation function of the weighted residuals. Buffer conditions were identical to those described above for the UV melting experiments. Fluorescence decays were fit to the following sum of exponentials:

$$I(t) = \sum_{i=1}^{3} \alpha_i e^{-t/\tau_i} \quad (1)$$

In this relationship, the values of α_i are the amplitudes of each component and the values of τ_i are the fluorescence lifetimes. Amplitude-weighted lifetimes ($\bar{\tau}$) were calculated from the following equation:

$$\bar{\tau} = \frac{\sum_{i=1}^{3} \alpha_i \tau_i}{\sum_{i=1}^{3} \alpha_i} \quad (2)$$

Isothermal Titration Calorimetry. Isothermal titration calorimetric (ITC) measurements were performed at 25 °C on a MicroCal VP-ITC (MicroCal, Inc.; Northampton, MA). Aliquots (10 μL) of paromomycin were injected from a 250 μL rotating syringe (300 rpm) into an isothermal sample chamber containing 1.42 mL of *Ec*WT or A1408G RNA solutions. The drug and RNA strand concentrations were 250 and 10 μM in the *Ec*WT experiment, while being 500 and 20 μM in the A1408G experiment. Each experiment was accompanied by the corresponding control experiment in which 10 μL aliquots of the drug were injected into a solution of buffer alone. The duration of each injection was 10 s and the initial delay prior to the first injection was 60 s. For the *Ec*WT experiment, the delay between injections was 240 s, while being 300 s for the A1408G experiment. Each injection generated a heat burst curve (microcalories per second vs seconds). The area under each curve was determined by integration [by use of the Origin version 7.0 software (MicroCal, Inc.; Northampton, MA)] to obtain a measure of the heat associated with that injection. The heat associated with each drug−buffer injection was subtracted from the corresponding heat associated with each drug−RNA injection to yield the heat of drug binding for that injection. Solution conditions were 10 mM sodium cacodylate (pH 5.5), 0.1 mM EDTA, and sufficient NaCl to bring the total Na^+ concentration to 150 mM.

(11) Szabo, A. G. In *Spectrophotometry & Spectrofluorimetry*; Gore, M. G., Ed.; Oxford University Press: New York, 2000; pp 33−67.

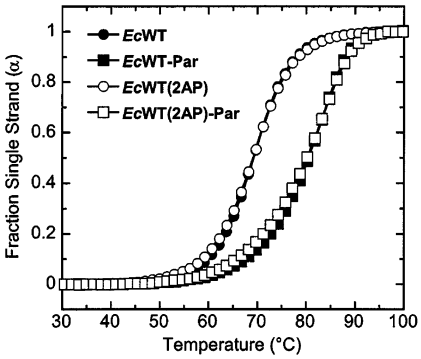

Figure 2. UV melting profiles for the *Ec*WT and *Ec*WT(2AP) duplexes, as well as for their paromomycin (Par) complexes {at a [drug]/[duplex] ratio (r_{dup}) of 1}. For clarity of presentation, the melting curves were normalized by subtraction of the upper and lower baselines to yield plots of fraction single strand (α) versus temperature.[22] All UV melting profiles were acquired at a wavelength of 274 nm. Solution conditions were 10 mM sodium cacodylate (pH 5.5), 0.1 mM EDTA, and sufficient NaCl to bring the total sodium ion concentration to 60 mM.

Results and Discussion

Thermal Denaturation Studies Reveal That the A1492-(2AP) Substitution Perturbs neither the Stability of *Ec*WT nor Its Affinity for Paromomycin. An important criterion that must be met when a fluorescent label is introduced into any biomolecule is that the structure and stability of the biomolecule be minimally perturbed as a result of the modification. In this connection, we selected A1492 as the base for 2AP substitution, due to its lack of involvement in any base-pairing interactions. We used temperature-dependent absorption spectroscopy to explore the impact of this substitution on the thermal stability of *Ec*WT and its paromomycin complex. Figure 2 shows the UV melting profiles for the *Ec*WT and *Ec*WT(2AP) duplexes, as well as for their paromomycin complexes. Note that the *Ec*WT and *Ec*WT(2AP) duplexes exhibit identical thermal stabilities, with melting temperatures (T_m) of 69.2 °C. Thus, the A1492(2AP) substitution does not perturb the thermal stability of the host RNA duplex. Further note that paromomycin binding enhances the thermal stabilities of the *Ec*WT and *Ec*WT(2AP) duplexes to similar extents, with the T_m values of the paromomycin complexes of *Ec*WT and *Ec*WT(2AP) being 80.5 and 80.2 °C, respectively. In other words, as measured by differences in T_m, the A1492(2AP) substitution does not alter the affinity of paromomycin for the host RNA.

Impact of Paromomycin Binding on the Steady-State Fluorescence of *Ec*WT(2AP) and A1408G(2AP) Is Consistent with Binding-Induced Base Destacking in the Former but Not the Latter Duplex. Figure 3 presents the steady-state fluorescence emission spectra of *Ec*WT(2AP) and A1408G-(2AP) in the presence and absence of paromomycin or guanidine hydrochloride. The binding of paromomycin to *Ec*WT(2AP) induces a marked increase in the fluorescence intensity of the RNA (Figure 3A). By contrast, paromomycin binding does not significantly alter the fluorescence of A1408G(2AP) (Figure 3B). We quantified the paromomycin-induced changes in the

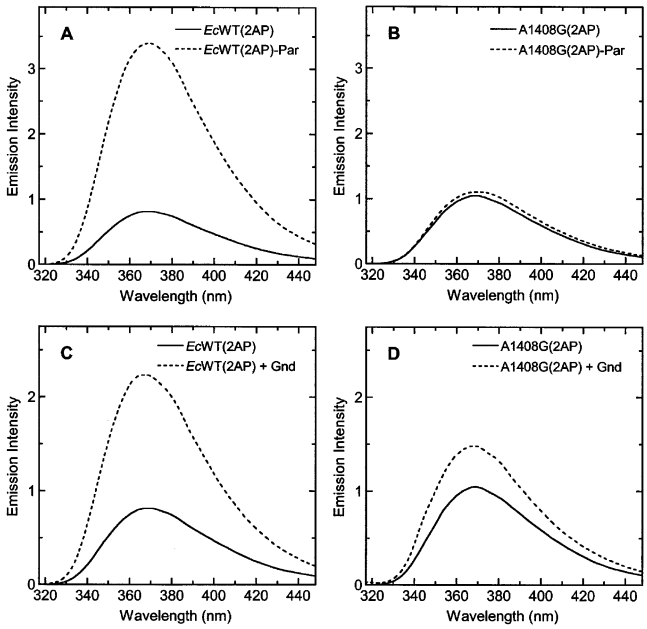

Figure 3. Steady-state fluorescence emission spectra at 25 °C of the *Ec*WT-(2AP) (A, C) and A1408G(2AP) (B, D) duplexes in the presence (dashed lines) and absence (solid lines) of paromomycin (Par) (A, B) or 6 M guanidine hydrochloride (Gnd) (C, D). The solution conditions were as described in the caption to Figure 2.

Table 1. Steady-State and Time-Resolved Fluorescence Parameters for *Ec*WT(2AP), A1408G(2AP), and Their Paromomycin Complexes at 25 °C

sample	Φ (±0.001)	$\bar{\tau}$[a] (ns)	$f_{stacked}$ [b]
r2AP	0.74[c]	10.7[c]	0
*Ec*WT(2AP)	0.030	1.13 ± 0.07	0.62 ± 0.04
*Ec*WT(2AP)-Par	0.077	2.09 ± 0.10	0.47 ± 0.04
A1408G(2AP)	0.076	3.01 ± 0.15	0.64 ± 0.02
A1408G(2AP)-Par	0.063	2.68 ± 0.14	0.66 ± 0.02

[a] The $\bar{\tau}$ values for *Ec*WT(2AP), A1408G(2AP), and their paromomycin complexes (calculated from eq 2) represent averages of at least three independent experiments, with the indicated uncertainties reflecting the standard deviations from the mean. [b] Values of $f_{stacked}$ were calculated from eq 3, with the indicated uncertainties reflecting the maximum possible errors as propagated through eq 3. The value of $f_{stacked}$ for r2AP is 0 by definition. [c] Values of Φ and $\bar{\tau}$ for r2AP were taken from Tsujikawa et al.[13]

steady-state fluorescence of *Ec*WT(2AP) and A1408G(2AP) in the form of quantum yields (Φ), which are listed in Table 1. Paromomycin binding to *Ec*WT(2AP) resulted in an increase of Φ from 0.030 ± 0.001 to 0.077 ± 0.001. By contrast, paromomycin binding to A1408G(2AP) resulted in a decrease of Φ from 0.076 ± 0.001 to 0.063 ± 0.001. These observations agree with the structural database (Figure 1) in being consistent with the binding-induced destacking of the base at position 1492 only when *Ec*WT(2AP), but not when A1408G(2AP), serves as the host duplex.[4,5,8] In fact, our steady-state fluorescence data suggest that when A1408G(2AP) serves as the host duplex, paromomycin binding actually enhances the stacking of the 1492 base. Note that the fluorescence intensities of both *Ec*WT(2AP) and A1408G(2AP) also increase upon denaturation with guanidine hydrochloride (panels C and D of Figure 3), supporting our correlation of paromomycin-induced changes in RNA fluorescence with corresponding changes in base stacking.

Quantifying the Extent of Drug-Induced RNA Base Destacking by a Combination of Steady-State and Time-Resolved Fluorescence Spectroscopy. Combining fluorescence quantum yield (Φ) and lifetime (τ) information allows one to quantify the extent of base stacking by calculating the fraction of intrahelical stacked base ($f_{stacked}$) with the following relationship:[12]

$$f_{stacked} = 1 - \Phi_{rel}/\bar{\tau}_{rel} \quad (3)$$

In this relationship, Φ_{rel} (=Φ/Φ_{r2AP}) and $\bar{\tau}_{rel}$ (=$\bar{\tau}/\bar{\tau}_{r2AP}$) are the quantum yield and amplitude-weighted fluorescence lifetime of 2AP in the RNA or paromomycin−RNA complex relative to the free riboside (r2AP). Barkley and co-workers[13] have previously reported Φ and $\bar{\tau}$ values for r2AP of 0.74 and 10.7 ns, respectively. By definition, the value of $f_{stacked}$ for r2AP is 0. We characterized the time dependence of the fluorescence intensities of *Ec*WT(2AP), A1408G(2AP), and their paromomycin complexes. A sample set of fluorescence decays that emerged from these measurements are shown in Figure 4. Global analyses of these decays with eq 1 yields the decay parameters (τ_i and α_i) listed in Table 2. Note that the decays for both *Ec*WT-(2AP) and A1408G(2AP), as well as their paromomycin complexes, can be described by the sum of three exponential terms. The Barkley and Ross groups have also observed three exponential fluorescence decays for a variety of different 2AP-substituted RNA and DNA duplexes,[12,13] with the corresponding fluorescence lifetimes being similar in magnitude to those reported here (Table 2).

The decay parameters listed in Table 2, as well as the corresponding decay parameters derived from at least two other independent experiments, were analyzed with eq 2 to yield the average $\bar{\tau}$ values listed in Table 1. Inspection of these values reveals that paromomycin binding increases the $\bar{\tau}$ value of *Ec*WT(2AP) from 1.13 to 2.09 ns, while minimally affecting the $\bar{\tau}$ value of A1408G(2AP) [the drug-induced change in the $\bar{\tau}$ of A1408G(2AP) is essentially within the experimental uncertainty]. Values of $\bar{\tau}$ provide a measure of dynamic quenching efficiency, which, for 2AP, results from collisions with nearby bases. The paromomycin-induced increase in the $\bar{\tau}$ value of *Ec*WT(2AP) is consistent with a corresponding decrease in dynamic quenching efficiency. One potential explanation for this observation is that the 2AP residue has a reduced range of motion in the drug−RNA complex compared to the drug-free RNA. Alternatively, the range of motion of the 2AP residue may be similar, or even greater, in the drug−RNA complex relative to the drug-free RNA, with the distance between the 2AP and nearby bases being greater in the complex than in the RNA alone. We favor the latter explanation, since the calculations described below, as well as the structural studies discussed above (see Figure 1), reveal a binding-induced destacking of the 1492 base, which, in turn, increases the distance between this residue and its neighbors.

The Φ and $\bar{\tau}$ values for *Ec*WT(2AP), A1408G(2AP), and their paromomycin complexes were used in conjunction with eq 3 to determine values of $f_{stacked}$. The results of these calculations are summarized in Table 1. Note that when *Ec*WT(2AP) serves as the host duplex, paromomycin binding decreases $f_{stacked}$ from 0.62 ± 0.04 to 0.47 ± 0.04. By contrast, paromomycin binding to A1408G(2AP) does not significantly alter $f_{stacked}$, with the drug-induced change in $f_{stacked}$ being within the experimental

(12) Rachofsky, E. L.; Seibert, E.; Stivers, J. T.; Osman, R.; Ross, J. B. A. *Biochemistry* **2001**, *40*, 957−967.
(13) Tsujikawa, L.; Strainic, M. G.; Watrob, H.; Barkley, M. D.; deHaseth, P. L. *Biochemistry* **2002**, *41*, 15334−15341.

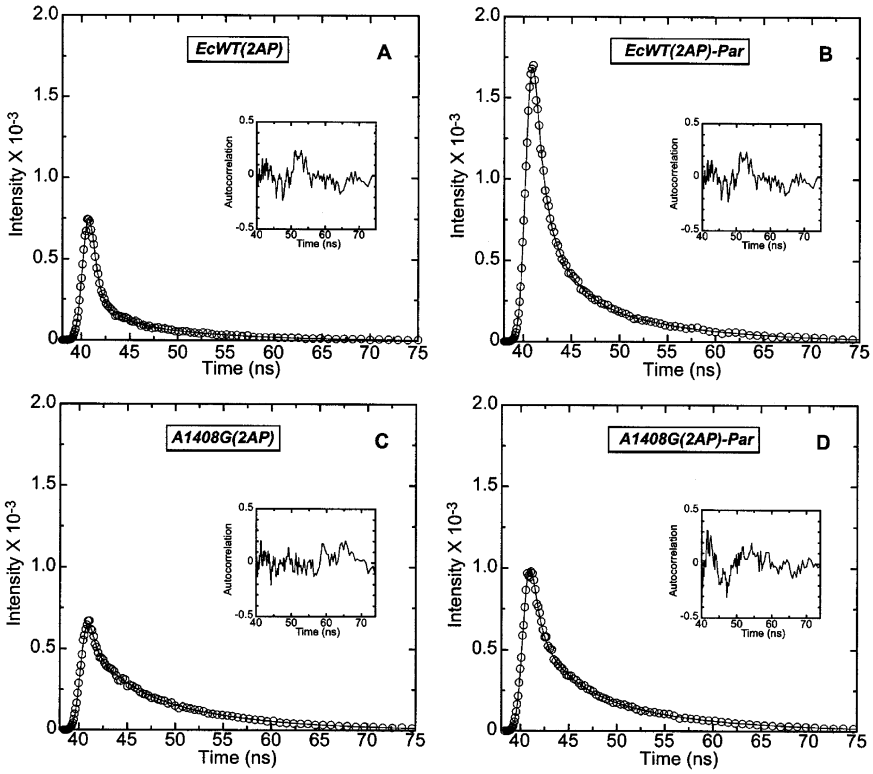

Figure 4. Time-resolved fluorescence decay profiles at 25 °C for the *Ec*WT(2AP) (A) and A1408G(2AP) (C) duplexes, as well as for their paromomycin (Par) complexes (at an r_{dup} ratio of 1) (B, D). In each panel, the open circles represent the experimental data points, while the solid lines reflect the nonlinear least-squares fits of the data with eq 1. The inset in each panel shows the autocorrelation function of the weighted residuals for the fit of the corresponding decay profile. The solution conditions were as described in the caption to Figure 2.

Table 2. Fluorescence Decay Parameters for *Ec*WT(2AP), A1408G(2AP), and Their Paromomycin Complexes at 25 °C[a]

sample	α_1	τ_1 (ns)	α_2	τ_2 (ns)	α_3	τ_3 (ns)	χ^2
*Ec*WT(2AP)	0.040 ± 0.001	8.83 ± 0.03	0.059 ± 0.001	2.27 ± 0.01	0.567 ± 0.002	0.414 ± 0.001	1.304
*Ec*WT(2 AP)-Par	0.098 ± 0.004	10.80 ± 0.19	0.252 ± 0.010	3.04 ± 0.13	0.763 ± 0.009	0.730 ± 0.024	1.242
A1408G(2AP)	0.104 ± 0.005	9.35 ± 0.17	0.057 ± 0.003	3.32 ± 0.37	0.243 ± 0.012	0.440 ± 0.032	1.271
A1408G(2AP)-Par	0.099 ± 0.005	10.11 ± 0.18	0.106 ± 0.004	3.48 ± 0.26	0.362 ± 0.009	0.657 ± 0.033	1.323

[a] For each RNA or drug−RNA complex, values of α_i, τ_i, and χ^2 were derived from global analysis of 10 decay curves by eq 1. The indicated uncertainties reflect the standard deviations of the experimental data from the fitted curves. Solution conditions were 10 mM sodium cacodylate (pH 5.5), 0.1 mM EDTA, and sufficient NaCl to bring the total sodium ion concentration to 60 mM.

uncertainty. In other words, paromomycin binding increases the average number of *Ec*WT(2AP) molecules in which the 2AP at position 1492 is destacked by 15%, while exerting little or no influence on the stacking of 2AP1492 in A1408G(2AP) molecules. This result is consistent with the NMR-derived structures[4,5,8] of the *Ec*WT and A1408G duplexes and their paromomycin complexes (see Figure 1). Thus, $f_{stacked}$ can provide a quantitative measure for the detection and characterization of the conformational change in the host rRNA induced by aminoglycoside complexation.

Implications with Regard to the Prokaryotic Specificity of Aminoglycoside Antibiotic Action. Eukaryotic ribosomes (including human ribosomes), which contain a guanine at position 1408 instead of the adenine that is present in prokaryotic ribosomes, are known to be resistant to the deleterious effects of aminoglycosides.[14] Similarly, prokaryotic ribosomes whose 16S rRNA carry the A1408G mutation also are resistant to aminoglycosides.[15] The aminoglycoside-resistant phenotype associated with G1408 correlates well with our observed aminoglycoside-induced changes in $f_{stacked}$ ($\Delta f_{stacked}$). This correlation is consistent with the notion that the drug-induced conformational change in the rRNA is an important determinant in the disruption of protein synthesis as well as the antimicrobial activities of 2-DOS aminoglycosides, while also highlighting the potential of $\Delta f_{stacked}$ to serve as a useful predictor of antibiotic activity.

Differential RNA binding affinities may also play a role in dictating the differential sensitivities of prokaryotic and A1408G-containing ribosomes to aminoglycosides. To address this possibility, we used isothermal titration calorimetry (ITC) to characterize the binding of paromomycin to *Ec*WT and A1408G duplexes. We have previously reported that aminoglycoside binding to *Ec*WT at pH > 5.5 is thermodynamically linked to drug protonation.[16,17] We conducted our comparative ITC studies of paromomycin binding to *Ec*WT and A1408G duplexes at pH 5.5, thereby eliminating contributions to the observed binding energetics from binding-linked drug protonation reac-

(14) Wilhelm, J. M.; Pettitt, S. E.; Jessop, J. J. *Biochemistry* **1978**, *17*, 1143−1149.
(15) Recht, M. I.; Puglisi, J. D. *Antimicrob. Agents Chemother.* **2001**, *45*, 2414−2419.
(16) Kaul, M.; Pilch, D. S. *Biochemistry* **2002**, *41*, 7695−7706.
(17) Kaul, M.; Barbieri, C. M.; Kerrigan, J. E.; Pilch, D. S. *J. Mol. Biol.* **2003**, *326*, 1373−1387.

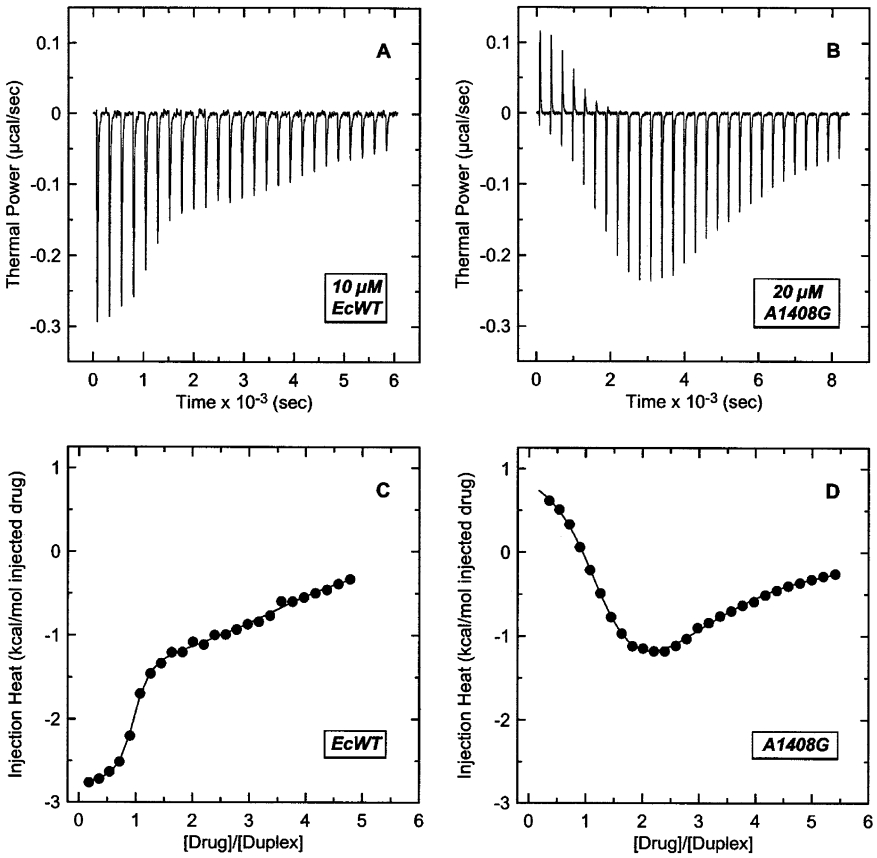

Figure 5. ITC profiles at 25 °C for the titration of paromomycin into a solution of *Ec*WT (A, C) and A1408G (B, D). Each heat burst curve in panels A and B is the result of a 10 μL injection of drug into a solution of RNA. The drug and RNA strand concentrations were 250 and 10 μM in the *Ec*WT experiment, while being 500 and 20 μM in the A1408G experiment. Solution conditions were 10 mM sodium cacodylate (pH 5.5), 0.1 mM EDTA, and sufficient NaCl to bring the total Na^+ concentration to 150 mM. The corrected injection heats shown in panels C and D were derived by integration of the corresponding heat burst curves shown in panels A and B, followed by subtraction of the corresponding dilution heats derived from control titrations of drug into buffer alone. The data points in panels C and D reflect the corrected experimental injection heats, while the solid lines reflect the calculated fits of the data via a model for two independent sets of binding sites.

Table 3. ITC-Derived Binding Parameters at 25 °C for the Complexation of Paromomycin with the *Ec*WT and A1408G Model Oligomers at pH 5.5 and a Na^+ Concentration of 150 mM[a]

RNA	K_1 (M^{-1})	ΔH_1 (kcal/mol)	N_1	K_2 (M^{-1})	ΔH_2 (kcal/mol)	N_2
*Ec*WT	$(3.7 \pm 0.7) \times 10^7$	-2.8 ± 0.1	0.9 ± 0.1	$(2.6 \pm 0.5) \times 10^5$	-1.4 ± 0.1	3.0 ± 0.1
A1408G	$(1.2 \pm 0.3) \times 10^6$	$+1.1 \pm 0.1$	1.2 ± 0.1	$(7.4 \pm 0.9) \times 10^4$	-3.0 ± 0.4	1.8 ± 0.2

[a] The values of K, ΔH, and N listed here were derived from the fits of the ITC profiles shown in panels C and D of Figure 5 with a model for two sets of independent binding sites. The indicated uncertainties reflect the standard deviations of the experimental data from the fitted curves (depicted as solid lines in panels C and D of Figure 5).

tions. The ITC profiles emerging from these studies are shown in Figure 5. Each of the heat burst curves in panels A and B of Figure 5 corresponds to a single drug injection. The areas under these heat burst curves were determined by integration to yield the associated injection heats. These injection heats were corrected by subtraction of the corresponding dilution heats derived from the injection of identical amounts of drug into buffer alone. Panels C and D of Figure 5 show the resulting corrected injection heats plotted as a function of the [drug]/[duplex] ratio. Note that the ITC profiles for the binding of paromomycin to *Ec*WT and A1408G are both biphasic, consistent with the presence of two binding equilibria. In each case, the first phase is significantly steeper than the second, an observation indicating that the binding constant (K) for the first equilibrium is greater than that for the second. We have previously assigned the first binding equilibrium to the specific A-site interaction observed in structural studies and the second binding equilibrium to weaker nonspecific interactions.[16,17]

The ITC profiles shown in panels C and D of Figure 5 were fit with a model for two independent sets of binding sites, with the binding parameters derived from these fits being summarized in Table 3. Inspection of these data reveals several features worthy of note: (i) For both *Ec*WT and A1408G, the first binding equilibrium is associated with a binding stoichiometry (N) of approximately 1 drug molecule/duplex, with the second binding equilibrium being associated with N values of 2−3 drug molecules/duplex. (ii) When *Ec*WT serves as the host duplex, K_1 (the binding constant associated with the first binding equilibrium) is approximately 142-fold greater than K_2 (the binding constant associated with the second binding equilibrium). Similarly, when A1408G serves as the host duplex, K_1 is approximately 16-fold greater than K_2. (iii) The enthalpy associated with the first binding equilibrium (ΔH_1) is exothermic (favorable) when *Ec*WT serves as the host duplex ($\Delta H_1 = -2.8 \pm 0.1$ kcal/mol) while being endothermic (unfavorable) when A1408G serves as the host duplex ($\Delta H_1 = +1.1 \pm 0.1$ kcal/

Table 4. Thermodynamic Profiles at 25 °C for the Binding of Paromomycin to the *Ec*WT and A1408G Model Oligomers at pH 5.5 and a Na^+ Concentration of 150 mM

RNA	ΔH^a (kcal/mol)	$T\Delta S^b$ (kcal/mol)	ΔG^c (kcal/mol)	K^a (M^{-1})
*Ec*WT	-2.8 ± 0.1	$+7.5 \pm 0.2$	-10.3 ± 0.1	$(3.7 \pm 0.7) \times 10^7$
A1408G	$+1.1 \pm 0.1$	$+9.4 \pm 0.2$	-8.3 ± 0.1	$(1.2 \pm 0.3) \times 10^6$

[a] Values of ΔH and K reflect the corresponding values of ΔH_1 and K_1 listed in Table 3. [b] Values of $T\Delta S$ were determined from eq 5, with the indicated uncertainties reflecting the maximum possible errors as propagated through eq 5. [c] Values of ΔG were determined from eq 4, with the indicated uncertainties reflecting the maximum possible errors as propagated through eq 4.

mol). Thus, the A1408G substitution confers an enthalpic penalty to the RNA binding of paromomycin, with this penalty being 3.9 kcal/mol in magnitude. (iv) The K_1 value for paromomycin−*Ec*WT complexation [$(3.7 \pm 0.7) \times 10^7$ M^{-1}] is approximately 31-fold greater than the corresponding value [$(1.2 \pm 0.3) \times 10^6$ M^{-1}] for paromomycin−A1408G complexation. In other words, paromomycin binds to the *Ec*WT duplex with a ∼31-fold higher affinity than A1408G. Thus, the A1408G substitution reduces paromomycin affinity for the rRNA A site.

The calorimetric data summarized in Table 3 allowed us to derive complete thermodynamic profiles for the binding of paromomycin to the *Ec*WT and A1408G duplexes. Specifically, we used the association constants derived from fits of our ITC profiles to calculate the corresponding binding free energies (ΔG) from the standard relationship

$$\Delta G = -RT \ln K \tag{4}$$

These calculated binding free energies, coupled with the binding enthalpies listed in Table 3, enabled us to calculate the corresponding entropic contributions to binding ($T\Delta S$) from the standard relationship

$$T\Delta S = \Delta H - \Delta G \tag{5}$$

The thermodynamic profiles resulting from these calculations are shown in Table 4. Note that the ∼31-fold higher affinity with which paromomycin binds the *Ec*WT relative to the A1408G duplex translates to a difference in ΔG of 2 kcal/mol. This differential binding affinity is enthalpic in origin. In fact, the enhanced binding of paromomycin to the *Ec*WT duplex occurs despite a less favorable entropic contribution to binding (+7.5 versus +9.4 kcal/mol), which is overcompensated by a more favorable binding enthalpy (−2.8 versus +1.1 kcal/mol). Thus, the 3.9 kcal/mol enthalpic penalty conferred by the A1408G substitution results in a 2.0 kcal/mol reduced affinity for the host RNA. In other words, paromomycin enthalpically distinguishes between the prokaryotic and eukaryotic rRNA sequence. The solution structures of paromomycin in complex with the *Ec*WT and A1408G duplexes (see panels C and D of Figure 1),[4,5,8] as well as our fluorescence results presented here, suggest that the molecular origins of the enthalpically driven 2.0 kcal/mol enhanced affinity of paromomycin for the prokaryotic versus the eukaryotic rRNA sequence are derived from the differing geometries of the two binding sites. These differing binding-site geometries are dictated by the identity of the base at the 1408 position. The A1408 base that is present in the prokaryotic sequence forms a noncanonical A·A pair with A1493,[5] with this pair being G1408·A1493 in the eukaryotic sequence.[8] From an energetic standpoint, the G·A pair is known to be more stable than the A·A pair.[18] This enhanced stability may confer too great an energetic barrier for drug-induced destacking of A1493 (and, in turn, A1492) in the eukaryotic sequence.

The reduced affinity of paromomycin for the eukaryotic versus prokaryotic rRNA sequence revealed by our calorimetric studies may be a determinant in the specificity of paromomycin for prokaryotic ribosomes. However, the affinity exhibited by paromomycin for the eukaryotic rRNA sequence [$(1.2 \pm 0.3) \times 10^6$ M^{-1}] is comparable to or even greater than those exhibited by other 2-DOS aminoglycoside antibiotics (e.g., tobramycin, kanamycins A and B, ribostamycin, and neamine) for the prokaryotic rRNA sequence under similar conditions.[16,17,19,20] Thus, RNA binding affinity alone does not appear sufficient to dictate the specificities and relative activities of aminoglycosides. It is likely that aminoglycoside-induced conformational changes in the host RNA also modulate these biological end points, perhaps to an even greater extent than RNA binding affinity.

Concluding Remarks

We describe here a method by which fluorescence can be used to detect and characterize changes in rRNA structure induced by drug complexation. Significantly, this method does not require that the drug be conjugated to a fluorescent molecule, which can alter RNA binding properties relative to the parent compound. Lynch and Puglisi[21] have reported an elegant NMR-based technique for detecting antibiotic-induced conformational changes in rRNA. Our fluorescence-based technique provides an alternative approach that is particularly useful when material and solubility are limiting factors. Furthermore, the fluorescent-based approach can be easily incorporated into a high-throughput regimen for the screening of both existing and novel compounds, with no chromophoric requirements on the part of these compounds. Finally, incorporation of anisotropy measurements into the methodology described here offers the potential of obtaining dynamic information (on a nanoscale time scale) about the drug-induced conformational change that is difficult to derive from the structural database alone.

Acknowledgment. We are indebted to Dr. Smita S. Patel for use of her PTI LaserStrobe fluorescence lifetime spectrometer. The calorimetric instrumentation was purchased through funds from NIH Grant S10 RR15959-01. This work was supported by grants from NIH (CA097123-01A1) and the American Cancer Society (RSG-99-153-04-CDD). C.M.B. was supported by an NIH training grant (5T32 GM 08319) in molecular biophysics.

JA030568I

(18) Turner, D. H. In *Nucleic Acids: Structures, Properties, and Functions*; Bloomfield, V. A., Crothers, D. M., Tinoco, I., Jr., Eds.; University Science Books: Sausalito, CA, 2000; pp 259−334.
(19) Wong, C.-H.; Hendrix, M.; Priestley, E. S.; Greenberg, W. A. *Chem. Biol.* **1998**, *5*, 397−406.
(20) Pilch, D. S.; Kaul, M.; Barbieri, C. M.; Kerrigan, J. E. *Biopolymers* **2003**, *70*, 58−79.
(21) Lynch, S. R.; Puglisi, J. D. *J. Am. Chem. Soc.* **2000**, *122*, 7853−7854.
(22) Marky, L. A.; Breslauer, K. J. *Biopolymers* **1987**, *26*, 1601−1620.